International Journal of Biological Macromolecules 365 (2026) 152376

Contents lists available at ScienceDirect

International Journal of Biological Macromolecules

journal homepage: www.elsevier.com/locate/ijbiomac

Alginate-based mucoadhesive nanofibrous system embedding resveratrol-loaded vesicles as a therapeutic platform for nasal disorders

Luca Casula [a], Michele Schlich [a], Elena Pini [b], Giovanna Rassu [c], Elena Bellotti [d], Francesco Lai [a], Maria Cristina Cardia [a], Salvatore Marceddu [e], Aurélien Dupont [f], Chiara Sinico [a], Carla Caddeo [a,*]

[a] Dept. of Life and Environmental Sciences, University of Cagliari, 09042, Monserrato, Cagliari, Italy
[b] Dept. of Pharmaceutical Sciences (DISFARM), University of Milan, 20133, Milan, Italy
[c] Dept. of Medicine, Surgery and Pharmacy, University of Sassari, Via Muroni 23/a, 07100, Sassari, Italy
[d] Dept. of Information Engineering, University of Pisa, Via G. Caruso 16, 56122, Pisa, Italy
[e] Institute of Sciences of Food Production – National Research Council, 07100, Sassari, Italy
[f] Biosit – UAR 3480, US_S 018, University of Rennes, F-35000, Rennes, France

ARTICLE INFO

Keywords:
Nanofibers
Mucoadhesive polymer
Green electrospinning
Phospholipid vesicles
Resveratrol
Nasal delivery

ABSTRACT

Oxidative stress and inflammation play a key role in the development and progression of several otorhinolaryngological disorders, including chronic rhinosinusitis and allergic rhinitis. Resveratrol (RSV), a natural polyphenol with antioxidant and anti-inflammatory properties, is a promising therapeutic candidate, although its clinical application is limited by poor aqueous solubility and rapid mucociliary clearance upon nasal administration.

In this study, a mucoadhesive nanofibrous nasal patch based on sodium alginate and poly(ethylene oxide) embedding RSV-loaded phospholipid vesicles was developed using a green electrospinning process based entirely on aqueous solvents. Both systems were characterized in terms of morphology, dimensional properties, swelling behavior, mucoadhesion, drug release, and biological activity.

The RSV vesicles showed nanoscale dimensions (~93 nm) and high entrapment efficiency (~88%). The combined system resulting from the incorporation of the RSV vesicles into the nanofibrous matrix exhibited remarkable swelling properties (up to ~800%), enhanced mucoadhesion, and a more sustained RSV release profile compared with vesicles alone, highlighting the role of the alginate network as a diffusion-controlling matrix.

In vitro studies in immortalized human keratinocytes confirmed excellent biocompatibility and enhanced antioxidant activity.

Overall, this vesicles-in-nanofibers platform represents a promising strategy for the nasal delivery of RSV, potentially improving its residence time and therapeutic effectiveness in upper airway diseases associated with oxidative stress and inflammation.

1. Introduction

Oxidative stress mediators, such as reactive oxygen species (ROS), play a dual role in inflammation. While they contribute to immune defense and tissue repair, they can exacerbate inflammation and lead to cellular damage. The imbalance between excessive ROS production and compromised antioxidant defenses results in the activation and release of inflammatory mediators (*i.e.*, cytokines, chemokines, *etc.*) that can further stimulate ROS production, creating a self-perpetuating cycle [1]. Recent research highlighted the critical role of the oxidant-antioxidant imbalance in the pathogenesis of otorhinolaryngological disorders, such as chronic rhinosinusitis and allergic rhinitis, showing high levels of oxidative stress markers that can contribute to nasal mucosa inflammation and reduce the epithelial barrier function [2]. Several compounds, such as vitamin C, vitamin E, and plant-extracted molecules, have been investigated as alternative therapeutic options for

* Corresponding author.
E-mail address: caddeoc@unica.it (C. Caddeo).

https://doi.org/10.1016/j.ijbiomac.2026.152376
Received 10 December 2025; Received in revised form 22 April 2026; Accepted 3 May 2026
Available online 5 May 2026
0141-8130/© 2026 The Authors. Published by Elsevier B.V. This is an open access article under the CC BY license (http://creativecommons.org/licenses/by/4.0/).

otorhinolaryngological diseases, with a large number of studies suggesting their potential to alleviate symptoms associated with oxidative stress [3,4]. Among these compounds, resveratrol (RSV) – a natural polyphenol abundantly present in red grape berry skins – has demonstrated antioxidant, anti-inflammatory and anti-allergic properties in chronic rhinosinusitis and allergic rhinitis [5–7]. Moreover, RSV can inhibit human rhinoviruses replication – the pathogen responsible for common colds – and regulate disrupted mucociliary clearance [8,9]. Despite RSV therapeutic potential, it has to be taken into account that the nasal delivery of antioxidant agents is often hindered by rapid mucociliary clearance, low residence time, and poor mucosal absorption. The nasal cavity has several protective mechanisms, such as mucus flow and ciliary activity, that rapidly remove exogenous substances, limiting the bioavailability and therapeutic efficacy of locally applied formulations [10]. Among the several approaches proposed to improve nasal drug delivery, the use of mucoadhesive polymers has led to increased residence time and, in some cases, permeation-enhancing properties [11]. Natural hydrophilic polymers are well known for their mucoadhesive properties, which are linked to their ability to swell and interact with nasal mucus, slowing down ciliary function, and increasing residence time [12,13]. This process can involve ionic bonds, covalent bonds, hydrogen bonding, Van der Waals forces, and hydrophobic interactions between the polymer chains and the mucin glycoproteins in the nasal mucus layer [14]. Using natural polymers to produce nanofibers – ultra-fine fibers with high surface area and porosity – represents a promising strategy to enhance nasal drug delivery by combining prolonged mucosal retention, biocompatibility and tunable drug release profiles [15]. Sodium alginate, an anionic polysaccharide derived from brown seaweed, known for its biocompatibility and gel-forming ability [12], has been extensively used in mucoadhesive nasal delivery systems, such as micro and nanoparticles [16–21]. Despite its extensive application in nanofiber systems for various administration routes [22–25], alginate-based nanofibers specifically designed for nasal drug delivery have not been studied yet. Only a limited number of studies have investigated nanofiber-based systems for nasal administration, even with other polymers. Most of these studies employ the nasal route for purposes other than treating localized nasal cavity diseases, but rather for vaccination purposes [26] or for the delivery of therapeutic agents, such as sedative–hypnotic [27] or antimigraine drugs [28], to the central nervous system. Only two studies have explored nanofiber-based systems for the local treatment of nasal disorders (*i.e.* rhinosinusitis), including pullulan-based nanofiber membranes co-loaded with ampicillin [29] and clove oil and mometasone furoate-loaded PLGA nanofibers [30]. This highlights an underexplored area with significant potential.

Therefore, the aim of this study was to design and produce a mucoadhesive patch made of alginate nanofibers – blended with a small percentage of poly(ethylene oxide) (PEO) to improve the spinnability of the formulation – for the nasal delivery of RSV, as a strategy to target oxidative stress/inflammation-associated otorhinolaryngological disorders. Since RSV is poorly water-soluble and susceptible to degradation, which combined with rapid metabolism, lead to very low bioavailability, it was first incorporated into phospholipid vesicles. The aqueous dispersion of vesicles was used as a medium to dissolve the hydrophilic alginate and PEO prior to electrospinning. By employing a green electrospinning approach that relies entirely on aqueous solvents, the proposed formulation ensures environmental compatibility and enhanced safety for mucosal applications [31]. Several studies have explored the combination of nanofibers and liposomes, highlighting the potential of this combined system for sustained drug delivery and improved drug bioavailability [32]. In a previous study, we demonstrated the efficient embedding of simvastatin-loaded liposomes in alginate-PEO nanofibers, which supports the feasibility of this strategy for hydrophobic drug delivery [33]. Based on this prior knowledge, we hypothesized that the combination of phospholipid vesicles and polymer nanofibers would result in a mucoadhesive formulation that enhances RSV bioavailability and residence time, while modulating its release in the nasal mucosa. The investigation of the systems' physico-chemical properties, swelling behaviors, release profiles, mucoadhesive properties, *in vitro* biocompatibility and antioxidant activity generated comprehensive evidence that supports the proposed hypothesis. To the best of our knowledge, this is the first study that investigates mucoadhesive alginate nanofibers embedding RSV vesicles for nasal delivery, broadening the applicability of polymer-based formulations in the biomedical field.

2. Materials and methods

2.1. Materials

Trans resveratrol (RSV, >99% pure, M.W. 228.25 g/mol) and polysorbate 80 (Tween 80, T80) were purchased from Galeno (Italy). Phospholipon® 90G (P90G, M.W. of approximately 776 g/mol), *i.e.* soybean phosphatidylcholine with a purity of minimum 94%, was supplied by Lipoid (Ludwigshafen, Germany). Polyethylene oxide (PEO; CAS 25322–68-3, product no. 372803, viscosity 2000–4000 cps at 2% in water, M.W. 2 MDa), sodium alginate (CAS 9005-38-3, product no. 180947, M.W. ~ 220 kDa – determined *via* Gel Permeation Chromatography (GPC; see section Supplementary Material) – and mannuronic acid to guluronic acid (M/G) ratio 1.50 ± 0.04 – determined *via* FTIR (see section 2.7.1), mucin (from pig stomach type II), 2′,7′-Dichlorodihydrofluorescein diacetate (DCFH-DA), phosphate buffered-saline (PBS), and sodium chloride (NaCl) were purchased from Merck (Rome, Italy). Potassium chloride was from Fluka Chemika (Buchs, Switzerland) and calcium chloride ($CaCl_2$) was from Riedel-de-Haën (Seelze, Germany).

Water was purified with a Milli-Q system with a 0.22 μm Millipak 40 filter (Millipore, Ireland). All other reagents were of analytical grade and were used as received, without any further purification or modification.

2.2. Vesicles preparation and characterization

RSV-loaded vesicles (RSV-ves) and empty vesicles (*E*-ves) were prepared using the direct sonication method [34]. Briefly, the components listed in Table 1 were dispersed in water and this dispersion was sonicated (5 s on, 2 s off, 8 cycles +5 s on, 2 s off, 3 cycles) using a high-intensity ultrasonic processor (Soniprep 150plus, MSE Crowley, London, UK).

Using a Zetasizer Nano (Malvern Panalytical, Worcestershire, UK), Dynamic Light Scattering (DLS) allowed the measurement of the vesicles' mean diameter and polydispersity index (PDI, an index of size distribution). A helium-neon laser (633 nm) was used to backscatter the samples at 174.7° and 25 °C. The M3-PALS (Mixed Mode Measurement-Phase Analysis Light Scattering) technique, which measures particle electrophoretic mobility, was used to estimate the zeta potential.

To evaluate the entrapment efficiency (EE%) of RSV-ves, 1 mL of sample was dialysed (Spectra/Por® membranes: 12–14 kDa M.W. cut-off, 3 nm pore size; Spectrum Laboratories Inc., DG Breda, The Netherlands) against 2 L of water for 2 h, in order to remove the RSV not incorporated into the vesicles. Both dialyzed and non-dialyzed samples were diluted (1:100 *v/v*) with methanol and analyzed by HPLC. The entrapment efficiency was calculated according to the following equation:

$$EE\ (\%) = \frac{RSV\ conc.(dialyzed\ sample)}{RSV\ conc.(non-dialyzed\ sample)}\ x\ 100 \quad (1)$$

2.3. HPLC analysis

RSV quantification was performed using an Alliance 2695 HPLC (Waters, Milan, Italy) connected to a photodiode array detector and a computer integrating system (Empower 3) using a previously validated method [35]. The samples were injected (10 μL) using a X-Select column

Table 1
Composition and characterization of the empty (*E*-ves) and RSV vesicles (RSV-ves; $n > 10$). D = mean diameter; PDI = Polydispersity Index; ZP = Zeta-potential; EE% = entrapment efficiency. Values are the means ± standard deviations (SD). ** = $p < 0.001$ and * = $p < 0.01$ *vs.* empty vesicles.

	Composition				Characterization			
	P90G (mg)	RSV (mg)	T80 (μL)	H_2O (μL)	D (nm ± SD)	PDI ± SD	ZP (mV ± SD)	EE (% ± SD)
E-ves	90	–	50	950	70 ± 5	0.18 ± 0.07	−21 ± 4	–
RSV-ves	90	5	50	950	93 ± 7**	0.17 ± 0.06	−24 ± 5*	88 ± 7

(RP18 3.5 μm, 4.6 × 150 mm; Waters), using methanol/acetonitrile/water/acetic acid (75/22.5/2.4/0.1 (*v/v*) as mobile phase at a constant flow rate of 0.8 mL/min and 306 nm as wavelength of detection. The calibration curve was built using a standard solution of RSV dissolved in methanol. The linear regression analysis, which produced a correlation coefficient value (R^2) of 0.999, was used to plot the calibration graphs. RSV retention time was 4 min, and the minimum detectable amount was 2 ng/μL.

2.4. Nanofibers preparation and characterization

A Linari Starter-kit (Linari Engineering srl, Pisa, Italy) was used to prepare the nanofibers by electrospinning. Briefly, to prepare the RSV vesicles-in-nanofibers (RSV-ves-nf), sodium alginate and PEO (weight ratio 75:25; total polymer concentration 4.2% (*w/w*)) were added to the RSV vesicle dispersion and stirred overnight at room temperature. The dispersion was then loaded into a plastic syringe, connected to a 21G stainless steel needle, and placed into a syringe pump. Electrospinning was carried out with a flow rate of 0.8 mL/h, and 16 kV voltage. The distance between the needle and the grounded flat collector was 17 cm, using a horizontal setup. To prepare the empty nanofibers (*E*-nf), the polymers were dissolved in water plus an amount of T80 equivalent to that used for the preparation of the vesicles.

The drug loading (DL) of RSV-ves-nf was evaluated by dissolving 20 mg of sample in 2 mL of a water/methanol mixture (1:1 *v/v*) using sonication to allow the complete dissolution of the nanofibrous mat. After analysing the samples by HPLC, DL was calculated according to Eq. 2:

$$DL\ (\%) = \frac{mass\ of\ RSV}{mass\ of\ nf}\ x\ 100 \quad (2)$$

The ratio of the experimental to theoretical drug content in the nanofibers was used to obtain the drug loading efficiency (DLE) (Eq. 3):

$$DLE\ (\%) = \frac{experimental\ DL}{theoretical\ DL}\ x\ 100 \quad (3)$$

2.5. Electron microscopy analysis

Cryogenic transmission electron microscopy (cryo-TEM) was used to study the vesicles' morphology. After deposition and blotting of 3 μL of each vesicle dispersion onto glow-discharged grids, they were frozen into ethane using an automatic plunge freezer (EM GP, Leica Microsystems Inc., Deerfield, IL, US). The vitrified samples were then observed under a 200 kV electron microscope (Tecnai G2 T20 Sphera, FEI Company/ThermoFisher Scientific, Waltham, MA, US), and a 4 k × 4 k CCD camera (TemCam-XF416, TVIPS GmbH, Gilching, Germany) was used to acquire the images using a setting of low electron dose and the camera in binning mode 1 and at a 25,000× magnification.

Scanning electron microscopy (SEM) was used to assess the nanofibers' morphology. The samples were electrospun in multiple layers onto aluminum foil, which was then cut and placed onto metallic stubs using double-side conductive tape. An environmental scanning electron microscope (Zeiss EVO LS 10, Oberkochen, Germany) running at 20 kV in high vacuum mode with a secondary electron detector [SEI] was used to observe samples without sputter coating at various magnifications. Using Image J 1.53 k software (National Institutes of Health, Bethesda, USA), the SEM images of at least 50 randomly chosen nanofibers were examined to determine the average diameter (d) and standard deviation (SD) [36].

2.6. Solid state characterization

The components used to prepare the formulations (RSV, P90G, T80, sodium alginate, PEO), their binary physical mixtures (PMs) with RSV (1:1 *w/w* = RSV:other component), *E*-ves, RSV-ves, E-nf and RSV-ves-nf were analyzed by Fourier Infrared Spectroscopy (FTIR), X-ray powder diffraction (XRPD) and Differential Scanning Calorimetry (DSC). PMs were prepared by properly weighing and mixing each component with RSV in a mortar. E-ves and RSV-ves were frozen at −30 °C and freeze-dried for 24 h using a Lyovapor L200 (Buchi, Cornaredo, Italy) to obtain solid powders.

2.6.1. FTIR analysis

The samples were placed on the ATR crystal for direct analysis using the attenuated total reflectance (ATR) mode with a diamond top-plate, in the range of 4000–650 cm^{-1}, on a Perkin Elmer Spectrum One FTIR (Perkin Elmer, Waltham, MA, USA). The equipment performed 4 scan pulses with a spectral resolution of 4 cm^{-1}. The sodium alginate FTIR spectra ($n = 3$) were used to determine the mannuronic acid to guluronic acid (M/G) ratio, based on the maximum absorbance of mannuronate O—H bending at 1024 cm^{-1} and guluronate C–O–C stretching at 1082 cm^{-1} [37].

2.6.2. XRPD analysis

Solid samples were placed into a sample holder and pressed to create a uniform and flat surface. XRD patterns of the pressed samples were recorded on a Rigaku MiniFlex X-ray diffractometer (Rigaku, Neu-Isenburg, Germany) equipped with a Cu Ka (k = 1.5406 Å) radiation source and operated at 30 kV/15 mA, in the range from 3 to 60 2θ, in steps of 0.02, using a scan step time of 2.00 s. The results were obtained as peak height (intensity) *vs.* 2 θ.

2.6.3. DSC analysis

The thermal behavior of the samples was investigated by differential scanning calorimetry using a Perkin Elmer DSC 4000 (Waltham, MA, USA), in nitrogen atmosphere (flow rate: 20 mL/min). The calibration was performed with metallic indium. The samples (approximately 2 mg) were pressed in aluminum pans and heated at a rate of 10 °C/min from 30 to 250 °C.

2.7. Release studies

RSV release from RSV-ves and RSV-ves-nf was evaluated in Simulated Nasal Fluid (SNF), using Franz vertical cells with a diffusion area of 0.785 cm^2 [38,39]. SNF was prepared by dissolving 7.45 g of NaCl, 1.29 g of KCl and 0.24 g of $CaCl_2$ in water (final volume: 1 L) and adjusting the pH to 6.4 with a pHmeter (Mettler Toledo FiveEasy™, Milan, Italy) [40]. A single layer of pre-hydrated Spectra/Por® membrane (12–14 kDa M.W. cut-off, 3 nm pore size) was placed between the donor and receptor compartments. Each formulation (130 μL of RSV-ves or 20 mg of RSV-ves-nf) was placed in the donor compartment onto the

membrane, and SNF was added to reach a final volume of 500 μL. The receptor compartment was filled with 6.2 mL of SNF + 1% (*w/v*) sodium dodecyl sulphate, which was used to ensure sink conditions. The cells were stirred at 300 rpm and thermostated at 37 ± 1 °C. At pre-determined timepoints (15 and 30 min, 1, 2, 4, 6, 8, 24, 30, 48, 54 and 72 h), 2 mL of the SNF medium was withdrawn from the receptor compartment, which was replenished with an equal volume of fresh medium. The withdrawn samples were analyzed by HPLC for RSV quantification (see Section 2.3).

2.8. Swelling assay

To evaluate the liquid absorbing capacity of the nanofibers, *E*-nf and RSV-ves-nf were cut in circular patches (0.79 cm^2) using a biopsy cutter, weighed (W_0), and placed in a 24-well tissue culture plate previously filled with 1 mL of SNF and incubated using a shaking incubator (37 °C, 50 rpm). At pre-determined timepoints (1, 2, 4, 8 h), the samples were retrieved, blotted with filter paper to remove excess SNF, and weighed (W_t) [41].

The percentage swelling ratio was determined using the following equation:

$$Swelling\ ratio\ (\%) = \frac{Wt - W0}{W0}\ x\ 100 \quad (4)$$

2.9. Mucoadhesion test

The mucoadhesion test was performed as previously described [42]. To test the liquid samples (*E*-ves and RSV-ves), a filter paper saturated with artificial nasal mucus (ANM) [43] was placed onto the surface of the probe with double-sided adhesive tape and 50 μL of each sample was applied between the two surfaces. For solid samples (E-nf and RSV-ves-nf), a circular patch obtained with a biopsy cutter (0.79 cm^2) was placed onto the surface of the probe with double-sided adhesive tape, whereas a filter paper saturated with ANM was placed on the base of the balance. A contact force of 10 g was applied for 120 s and the detachment force (in g) was measured. As a control, the test was performed using 50 μL of pure water - instead of the vesicle dispersions - or an aluminum foil (0.79 cm^2) - instead of the nanofibers. The mucoadhesive strength was expressed in mN/cm^2. The experiments were performed in triplicate (n = 3).

2.10. Biocompatibility

Spontaneously immortalized human keratinocytes (HaCaT, obtained by ATCC, Manassas, VA, US) were cultured in Dulbecco's Modified Eagle Medium (DMEM, high glucose, Corning, Corning, NY, US) containing 100 U/mL penicillin, 0.1 mg/mL streptomycin, 2 mM L-glutamine and 10% fetal bovine serum and maintained in a humidified incubator at 37 °C with 5% CO_2. The cells were seeded in 96-well plates (10^4 cells/well) and allowed to attach and grow for 24 h prior to exposure to formulations for an additional 24 h. Treatments were prepared as follows: dissolution and dilution in complete medium (RSV-ves-nf and *E*-nf); dilution with complete medium (RSV-ves and E-ves); dissolution in DMSO and dilution with complete medium (RSV). At the end of the treatments, the medium was replaced with a solution of MTT (3-(4,5-dimethyl-2-thiazolyl)-2,5-diphenyl-2H-tetrazolium bromide, Merck, Rome, Italy) in PBS (0.25 mg/mL). After 3 h, the MTT solution was replaced with ethanol to dissolve the formazan crystals, and absorbance was measured at 570 nm using a Synergy 4 plate reader (BioTek, Winooski, VT, US). The results are expressed as the percentage of metabolically active cells *vs.* untreated cells (100%) (average ± standard deviation, n = 5).

2.11. In vitro cellular antioxidant activity

The ability of RSV-containing formulations to protect cells from exogeneous oxidative stress was assessed using the intracellular reactive oxygen species (iROS) probe 2′,7′-dichlorodihydrofluorescein diacetate (DCFH-DA) [44]. HaCaT cells were seeded in 96-well plates (2×10^4 cells/well) and allowed to grow for 48 h. The cells were then exposed to formulations (or relevant controls) diluted in complete medium (final RSV concentration: 250 μg/mL) for 4 h. The treatments were followed by sequential incubation with DCFH-DA in PBS (30 min) and 350 μM hydrogen peroxide in PBS (120 min). At the end of the incubation time, the amount of iROS-oxidized probe was: (I) qualitatively observed by fluorescence microscopy using a Leica DM IL LED equipped with 20× objective and a MC170 HD camera controlled by LAS *v.* 4.12 software (Leica Mycrosystems Srl, Buccinasco, Italy); (II) quantitatively determined by fluorescence reading (480–530 nm) using a Synergy 4 plate reader. The percentage of iROS was calculated according to the following equation:

$$iROS\ (\%) = \frac{(F_t - F_{bkg}) \times 100}{(F_{ut} - F_{bkg})} \quad (5)$$

Where F_t: fluorescence of test well; F_{bkg}: background fluorescence of cells not exposed to DCFH-DA; F_{ut}: fluorescence of cells not exposed to treatments nor to hydrogen peroxide. The results are expressed as the average ± standard deviation (n = 5).

2.12. Statistical analysis

Data are presented as means ± standard deviations (SD). Multiple comparisons of means (one-way ANOVA, post-hoc Tukey HSD test) were used to substantiate statistical differences between the compared groups, while the Student's *t*-test was used to compare two samples. Data analysis was performed with the XL Statistic for Microsoft Excel software package. The significance level p was set to 0.05.

3. Results and discussion

In recent years, increasing attention has been devoted to nasal delivery strategies for RSV, aiming to overcome its poor aqueous solubility and limited bioavailability, while enabling local therapeutic action in the nasal cavity. These include nasal solutions incorporating resveratrol and carboxymethyl-β-glucan [45] designed to enhance mucosal protection and anti-inflammatory activity, or chitosan-coated solid lipid microparticles [46] for improving RSV stability and nasal residence time, or nanoemulsions co-loading luteolin and RSV incorporated in carboxymethyl chitosan [47] with synergistic antioxidant and anti-inflammatory activities. More advanced approaches have also been proposed, such as α-helical cell-penetrating peptide conjugation [48], which facilitates epithelial penetration and intracellular delivery of RSV.

Despite these advances, strategies combining improved RSV solubilization with prolonged nasal residence remain limited. Therefore, the aim of this study was to develop a mucoadhesive nanofiber-based system embedding RSV-loaded phospholipid vesicles for controlled nasal delivery.

3.1. Development of RSV-loaded vesicles

Empty and RSV-loaded vesicles were prepared using the direct sonication method. DLS analysis showed an average diameter of 70 nm for the *E*-ves. The addition of RSV caused an increase in vesicle diameter to 93 nm. Nevertheless, the PDI remained below 0.2, a value that indicates a narrow size distribution. A preliminary study (data not shown) revealed that the presence of Tween 80 − a nonionic hydrophilic surfactant widely used in food and pharmaceutical industries – was key to obtaining homogeneous, nanosized vesicles with the chosen RSV

concentration (5 mg/mL), as it played a crucial role in decreasing vesicle size, avoiding the formation of RSV precipitates and ensuring colloidal stability [49]. Moreover, given that the aim of this work was to produce nanofibers with embedded phospholipids vesicles, the addition of Tween 80 was also beneficial to reducing the surface tension of the polymer solutions for nanofibers production, optimizing the formation of the Taylor cone and resulting in a stable electrospinning process [50,51].

After purification of RSV-ves by dialysis, an entrapment efficiency of 88% was determined, which is in line with previous studies reported in the literature [52,53].

The morphology of RSV-ves was investigated *via* cryo-TEM. The micrograph in Fig. 1 highlights the presence of unilamellar vesicles below 100 nm in size.

3.2. Development of vesicles-in-nanofibers

Several alginate hybrid systems have already been studied for the delivery of RSV, such as alginate and graphene nanoplatelets beads [54], alginate-sucrose and alginate-chitosan microbeads containing liposomes [55] or gold nanoparticles functionalized with alginate [56]. These systems were developed mostly to improve RSV stability or to modulate its release profile and were not specifically intended for nasal administration. In addition, most of these formulations differ substantially from the proposed electrospun nanofibers in terms of architecture, surface area, and the ability to form mucoadhesive matrices capable of prolonging residence time in the nasal cavity.

In this study, sodium alginate was chosen for the preparation of nanofibers due to its high biocompatibility and mucoadhesive properties. Mucoadhesive polymers are known to increase drug retention in the nasal epithelium, improving the absorption of drugs with poor bioavailability [11]. Since alginate's polyelectrolyte nature and chain conformation make it difficult to electrospin, a blend polymer solution of sodium alginate and PEO was used [57].

In a previous study [33], we proved the feasibility of incorporating phospholipid vesicles into nanofibers as a strategy to obtain a highly concentrated polymer aqueous dispersion of a poorly water-soluble drug and to achieve a green electrospinning process [31].

In this study, preliminary experiments were conducted to evaluate the optimal polymer concentration (data not shown), which is known to be one of the key parameters to achieve a constant and stable electrospinning process [58]. A total polymer concentration of 4.2% (*w/w*) and a sodium alginate:PEO ratio of 75:25 were selected to produce the final formulation. SEM micrographs and diameter distribution of empty and RSV vesicles-in-nanofibers are shown in Fig. 2. Average diameters of nanofibers are reported in Table 2. *E*-nf appeared as a dense network of nanofibers with variable diameter (374 ± 160 nm) and beads, a morphology that can be described as “beads on a string”. A similar morphology was observed by Jeong et al. when preparing nanofibers with an alginate:PEO ratio of 80:20, which is close to the one used in this study [59]. RSV-ves-nf showed a more homogeneous morphology with less beads and irregularities, which resulted in lower average diameter and lower diameter distribution (314 ± 113 nm). It is widely known that nanofibers morphology, which can include beading, spindling, or fibers formation, is significantly influenced by the degree of chain entanglement in the liquid containing the polymer. Polymer chain entanglement for fibers formation requires a high molecular weight polymer and sufficient viscosity [60,61]. The different morphology observed for *E*-nf and RSV-ves-nf (“beads on a string” *vs.* almost beads-free) might be attributed to an increase in viscosity and chain entanglement due the

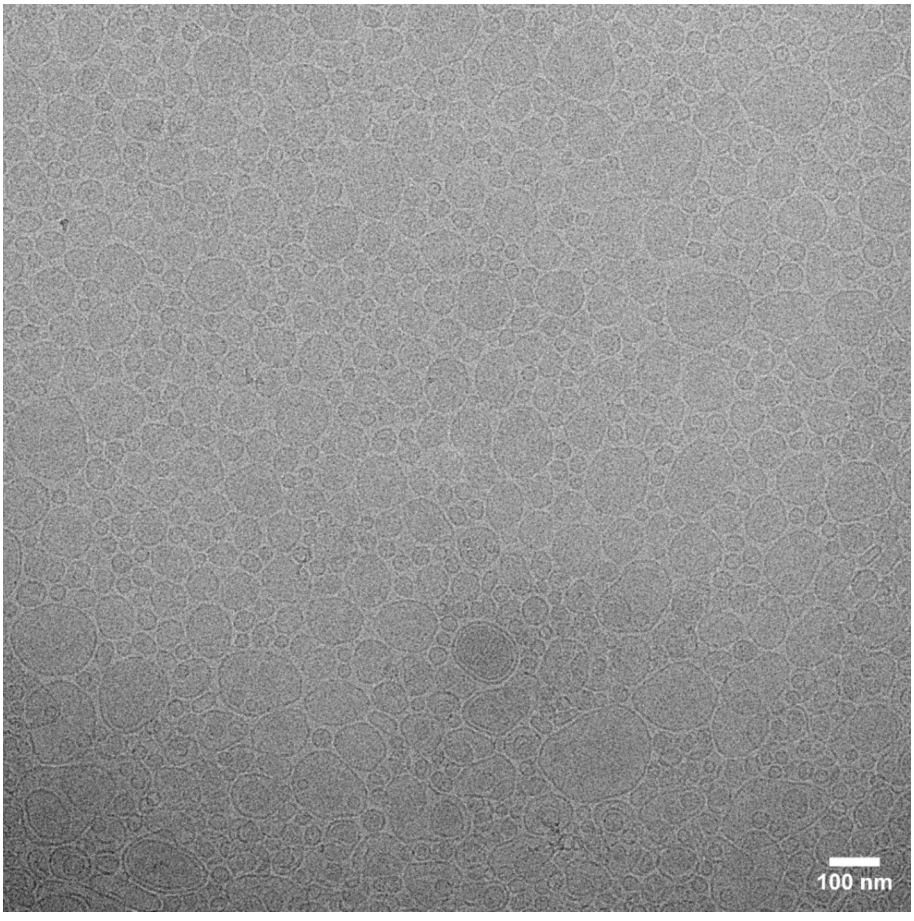

Fig. 1. Cryo-TEM micrograph of RSV-ves.

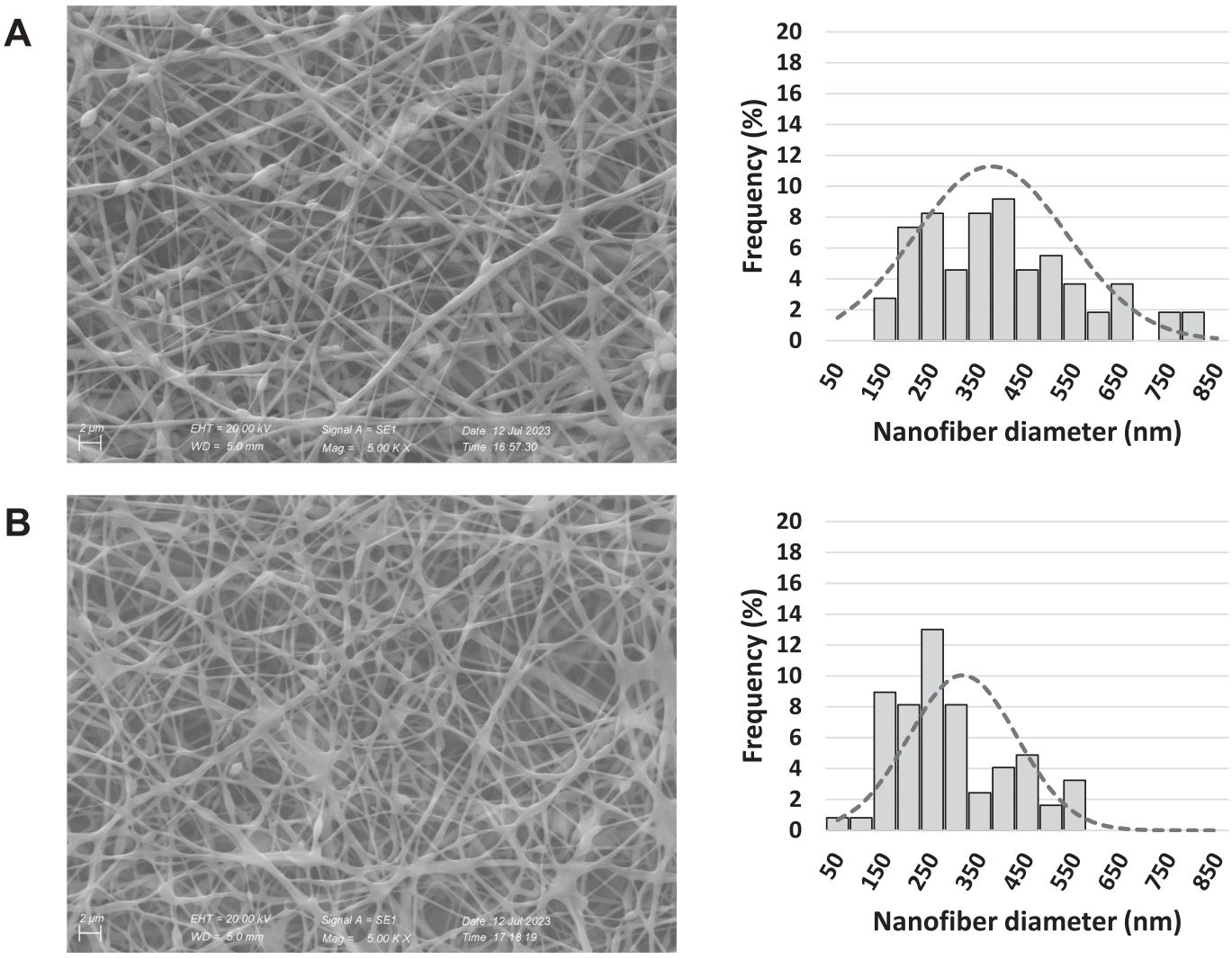

Fig. 2. SEM images and diameter distribution of A) *E*-nf and B) RSV-ves-nf.

Table 2
Characterization of empty nanofibers (E-nf) and RSV vesicles-in-nanofibers (RSV-ves-nf) in terms of average nanofiber diameter (nm), drug loading (DL, % w/w), and drug loading efficiency (DLE, %). (* = $p < 0.01$).

Samples	Nf diameter (nm)	DL (% *w/w*)	DLE (%)
***E*-nf**	374 ± 160 *	–	–
RSV-ves-nf	314 ± 113 *	2.3 ± 0.1	91.3 ± 5.0

presence of the phospholipids in RSV-ves-nf, as also reported by De Freitas Zômpero et al. when adding nanoliposomes to polyvinyl alcohol solutions for electrospinning [62].

The drug loading (DL) of the nanofibers was determined *via* HPLC. As can be seen in Table 2, the DL of RSV-ves-nf was 2.3% (*w/w*), with an entrapment efficiency (Drug Loading Efficiency, DLE) of 91%. These results confirm that the incorporation of RSV into phospholipid vesicles prior to electrospinning did not negatively affect the final RSV content in RSV-ves-nf.

3.3. Solid state characterization of vesicles and nanofibers

The FTIR study was performed to assess compatibility among the formulation components. The infrared spectra of raw materials were consistent with those found in the literature [63–66] and the spectra of 1:1 physical mixtures (PMs) exhibited peaks characteristics of each component, without the appearance of new bands (data not shown). Hence, chemical interactions between the components can be excluded.

The spectra of RSV, *E*-ves, RSV-ves, E-nf, and RSV-ves-nf are reported in Fig. 3A. The absorption peaks in RSV spectrum at 3193 and 3020 cm^{-1} were attributed to O—H stretching, at 3020 cm^{-1} to Csp^2-H stretching, at 1632, 1604 and 1583 cm^{-1} to the aromatic and aliphatic C═C stretchings, at 1159 and 1144 cm^{-1} to the C—O bond and at 829 cm^{-1} to the *trans* C═C vibrations. The spectrum of empty vesicles is the superimposition of P90G and Tween80 spectra, while in the FTIR of RSV vesicles specific peaks that lead back to RSV can be highlighted at 1603 (C═C bond), at 1167 and 1143 cm^{-1} (C—O bond). Since the spectra of E-nf and RSV-ves-nf differ only for the presence of the RSV peaks at 1167 and 1143 cm^{-1} and no new absorption peaks appeared, it can be assumed that there is no chemical interaction between components.

The XRPD pattern of RSV confirms its crystalline state [67] with sharp diffraction peaks at 2ϑ: 6.54, 16.28, 19.10, 22.24, 23.48, 25.14, 28.24°. RSV maintains its crystalline profile in the PMs, while it disappears in the vesicles, suggesting its efficient incorporation. Furthermore, the diffractogram of RSV-ves-nf showed an amorphous profile where the two weak diffraction peaks observed at 2ϑ 18.58 and 22.62° are both characteristic of PEO, confirming the amorphous state of RSV in the nanofibrous system (Fig. 3B).

The thermal behavior of the raw materials, PMs, vesicles, and nanofibers was then studied (**Supplementary Fig. 3**). The characteristic

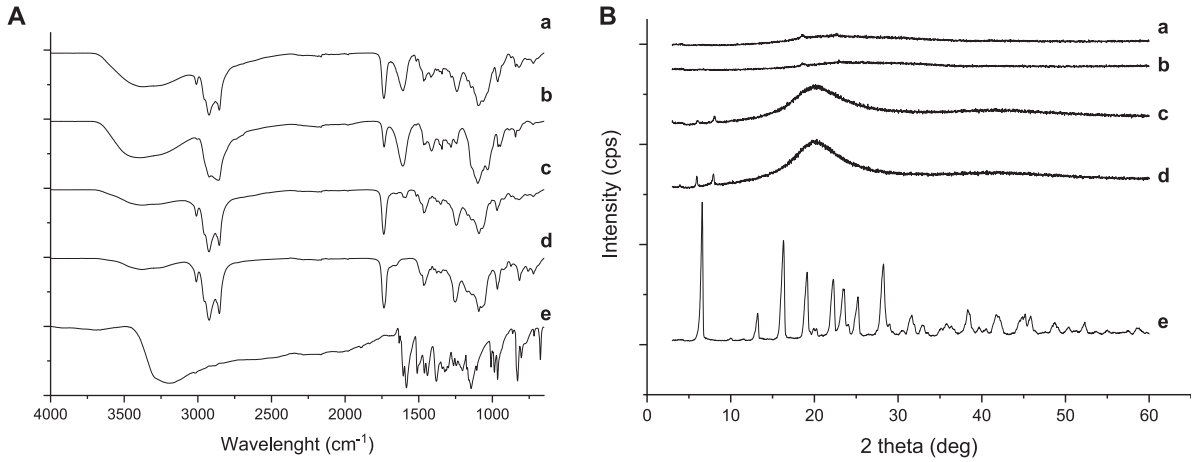

Fig. 3. A) FTIR, B) XRPD analysis of a) RSV-ves-nf, b) *E*-nf, c) RSV-ves, d) E-ves, e) RSV.

endotherm of RSV is seen at 267.02 °C [63], which corresponds to its melting point; P90G thermogram shows three weak peaks around 174, 183 and 187 °C, confirming its amorphous state, as depicted in the XRPD profile. Sodium alginate exhibits an endothermic event at about 70 °C and another exothermic above 250 °C, which correspond to the evaporation of hydration water molecules and the oxidative degradation of alginate, respectively [68]. PEO shows a sharp endothermic event at 71 °C. The endothermic event of RSV disappears in all the PMs, except for the one with sodium alginate, suggesting an interaction between RSV and the polymer. RSV vesicles show the absence of RSV melting endotherm, suggesting its incorporation into the lipid bilayer. The RSV endothermic peak is missing in the thermograms of RSV-ves-nf, proving its amorphous state in the nanofibrous system.

3.4. Release studies

RSV is well known for its poor water solubility (~0.03 mg/mL), which can affect its release and result in low bioavailability [69,70]. Therefore, *in vitro* release studies are essential to evaluating the quality and performance of the proposed nasal delivery system. Among the different methods reported in the literature, vertical Franz diffusion cells have often been employed to test nasal mucoadhesive formulations [71]. In this study, the ability of RSV-ves and RSV-ves-nf to release RSV in a simulated nasal fluid using a vertical Franz diffusion cell apparatus was assessed (Fig. 4).

The release profiles revealed distinct behaviors for the two formulations. RSV-ves showed a faster and overall higher release compared with RSV-ves-nf. At nearly all time points, the amount of RSV released from RSV-ves was significantly greater than that from RSV-ves-nf, except at the final time point where no statistical difference was observed. After 72 h, cumulative release reached approximately 47% for RSV-ves and 37% for RSV-ves-nf. Although further release might occur over longer time periods (> 72 h), such prolonged residence times are unlikely under physiological nasal conditions. Because the nasal mucosa is cleared rapidly, a drug formulation would typically be cleared from the nasal cavity long before the release process completes. Nasal residence time typically lasts 15–30 min for conventional nasal sprays and up to 4–6 h for mucoadhesive products [72]. Therefore, a 72-h timeframe was considered adequate to determine the release performance of the two formulations, ensuring a robust comparison.

The slower release observed for RSV-ves-nf can be attributed to the presence of the sodium alginate nanofibrous matrix. Alginate is known to absorb water and form a gel-like network, which can restrict vesicle mobility and act as a diffusion barrier, thereby promoting a more gradual drug release [73]. This property is particularly advantageous for nasal delivery, where rapid mucosal clearance represents a major limitation to drug absorption [74]. In addition, the mucoadhesive nature of alginate may prolong the residence time of the formulation within the nasal cavity, potentially enhancing drug availability and absorption [75]. Similar effects have been described by Dukovski et al., who reported prolonged dexamethasone release from lipid–alginate nanoparticles incorporated into a sprayable *in situ* forming pectin gel for nasal

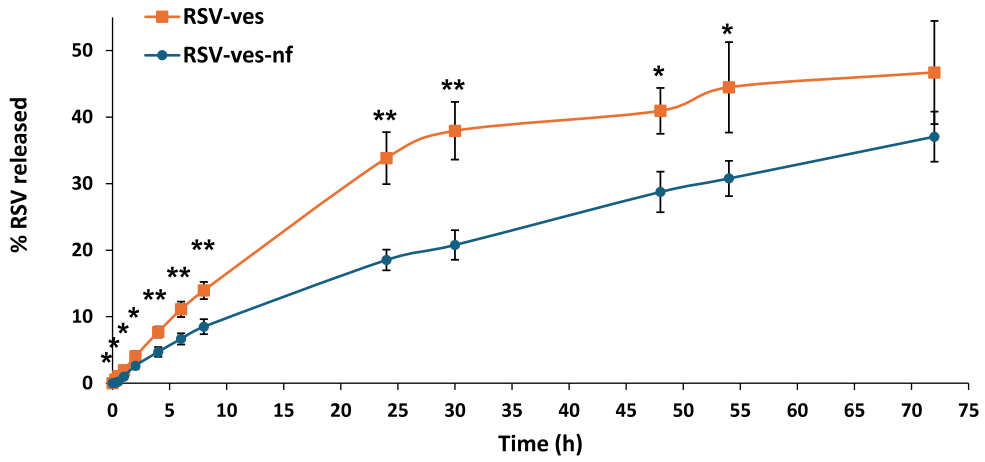

Fig. 4. Release profiles of RSV from RSV-ves and RSV-ves-nf in simulated nasal fluid at 37 °C, expressed as percentage (%) of drug released over 72 h ($n = 4$; * = $p < 0.05$; ** = $p < 0.01$ RSV-ves *vs.* RSV-ves-nf at the same time point).

administration [16].

Upon contact with the simulated nasal fluid, RSV-ves-nf likely undergo an initial hydration step in which the nanofibrous matrix absorbs fluid and swells, followed by gradual rehydration of the embedded vesicles. In contrast, RSV-ves are immediately exposed to the fluid, leading to a faster RSV release toward the receptor compartment. Accordingly, RSV-ves displayed a biphasic release pattern characterized by an initial burst phase followed by a slower release stage. The burst effect can be attributed to the rapid diffusion of non-incorporated RSV (approximately 12% of the total RSV content in the vesicle dispersion) as well as RSV molecules located near the phosphocholine headgroups of the vesicle bilayer [76]. Subsequently, the release rate decreases as RSV diffuses through the lipid bilayer before reaching the surrounding medium.

Conversely, the RSV-ves-nf exhibited a more sustained and gradual release profile, consistent with diffusion through a hydrated polymeric matrix. Other studies have reported similar controlled release from hybrid systems made of phospholipids vesicles embedded in polymeric nanofibers [77–79].

To further investigate the release mechanism, the experimental data were fitted to commonly used kinetic models, including the Higuchi and Korsmeyer–Peppas models. The release profile of RSV-ves-nf showed an excellent correlation with the Higuchi model ($R^2 = 0.996$), indicating that diffusion through a hydrated matrix is the predominant release mechanism. Analysis using the Korsmeyer–Peppas model (applied to the initial portion of the release curve) yielded a release exponent $n = 1.15$ ($R^2 = 0.95$), suggesting a non-Fickian transport mechanism dominated by polymer relaxation and matrix swelling, which is typical of hydrophilic polymer networks such as alginate nanofibers. This dual interpretation suggests that the release process is not purely diffusion-controlled, but it rather involves a dynamic interplay between matrix hydration, swelling, and structural rearrangement, which progressively modulates RSV mobility within the system.

From a physiological perspective, nasal drug delivery is strongly limited by mucociliary clearance, which typically removes formulations from the nasal cavity within approximately 10–20 min [80]. Therefore, although extended-release profiles over 72 h are useful for mechanistic comparison, the early release phase becomes particularly relevant for *in vivo* performance. In this context, the RSV-ves-nf offers a key advantage: the combination of rapid hydration and swelling with strong mucoadhesion may enhance nasal residence time, allowing the formulation to partially overcome mucociliary clearance and maintain close contact with the mucosa. Moreover, the absence of a pronounced burst effect and the more gradual release observed for RSV-ves-nf suggest a controlled bioavailability of RSV during the critical early time window. Notably, only approximately 1% of RSV was released in the first hour, confirming the absence of an initial burst and the strong retention of RSV within the nanofibrous matrix. This behavior may be advantageous in nasal delivery, as it allows the formulation to remain localized and gradually release a drug while benefiting from enhanced mucoadhesion and prolonged residence time. In contrast, the faster-releasing vesicle dispersion may lead to a more rapid RSV loss due to mucociliary clearance. This balance between initial retention and sustained release is particularly relevant for nasal applications, where both prolonged contact and controlled drug availability are required. This limited early release supports a retention-driven delivery mechanism rather than a burst-driven clearance, which is particularly advantageous in the context of nasal administration.

To correlate these *in vitro* findings with *in vivo* behavior and establish a possible dosing regimen, a comparison could be made with a currently available, marketed nasal product containing resveratrol, such as Zerinol Nasal Care® nasal spray (Zentiva), which contains approximately 0.5 mg/mL of RSV. RSV-ves-nf provided a gradual release of RSV over time - approximately 0.055 ± 0.007 mg within 8 h, which is comparable to the amount delivered by a single puff (roughly 130 μL) of the commercial spray. If a RSV-ves-nf patch were hypothetically applied 2–3 times per day, it would provide a similar amount of RSV over time, but with a controlled and sustained release profile, rather than having the rapid peak-and-clearance behavior typical of liquid formulations.

Therefore, although precise dosing regimens cannot be defined at this stage, the proposed RSV vesicles-in-nanofibers may enable a potential advantage toward prolonged nasal delivery that will need validation by *in vivo* studies.

3.5. Swelling and mucoadhesive properties

Mucoadhesion occurs in two key phases. In the first phase, upon contact with the mucous layer, the formulation undergoes a hydration-induced swelling process, which increases the mobility of polymer chains and promotes their interaction and entanglement with mucin. This ensures close contact between the polymer and mucus, a process influenced by several properties of the materials, such as wettability, swelling time, and hydration. In the second phase, moisture plasticizes the system enabling mucoadhesive particles to bind to mucin *via* hydrogen or van der Waals bonds [81].

To investigate the swelling and mucoadhesive properties of RSV-ves-nf, which can influence RSV release and residence time, *in vitro* tests were carried out (Fig. 5).

B) Mucoadhesive strength of empty and RSV vesicles (E-ves and RSV-

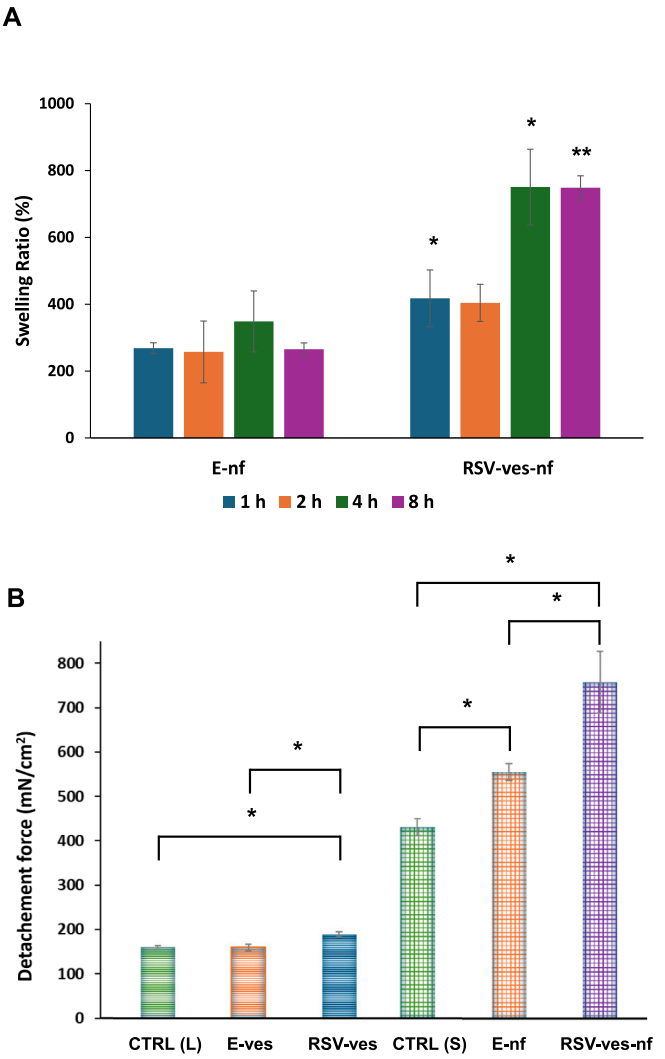

Fig. 5. A) Swelling properties of empty nanofibers (*E*-nf) and nanofibers embedding RSV vesicles (RSV-ves-nf). * = $p < 0.05$; ** = $p < 0.01$ RSV-ves-nf *vs.* *E*-nf at the same timepoint.

ves) and nanofibers (E-nf, RSV-ves-nf). * = $p < 0.05$ vesicles *vs.* liquid control (CTRL (L)); nanofibers *vs.* solid control (CTRL (S)).

The ability of the nanofibrous patch to absorb the simulated nasal fluid (SNF) and swell was evaluated at different timepoints (Fig. 5A). The remarkable swelling properties of sodium alginate are shown by the swelling ratio values of *E*-nf. Indeed, the swelling ratio was >200% after 2 h, reached its maximum at 4 h, and decreased at 8 h, which is in line with the observed partial erosion of the patch. RSV-ves-nf exhibited swelling ratios significantly higher ($p < 0.05$; Fig. 5A) than those of *E*-nf at almost all time points (except for 2 h). The swelling ratio of RSV-ves-nf was almost twice as that of E-nf after 1 h (400%), reached almost 800% after 4 h, and remained unchanged at 8 h, without evidence of erosion.

The mucoadhesion of the formulations was then assessed following a previously used method with artificial nasal mucus (ANM) [42,43], where liquid (water) or solid (aluminum foil) controls were used for vesicles or nanofibers, respectively. *E*-ves did not show a mucoadhesive strength statistically different from the corresponding liquid control ($p > 0.05$), whereas the mucoadhesive strength of RSV-ves (189.5 ± 6.6 mN/cm^2; Fig. 5B) was significantly higher than that of *E*-ves and the liquid control, suggesting a possible contribution of RSV in enhancing mucoadhesion. As expected, E-nf exhibited a mucoadhesive strength significantly higher than that of the vesicles and the solid control, attributable to sodium alginate [73], and RSV-ves-nf showed the highest value (761.7 ± 69.5 mN/cm^2; Fig. 5B). This result can be explained by the fact that RSV-ves-nf contain a high percentage of phospholipid vesicles (>50% *w/w*) that could reduce the water solubility of alginate – compared to E-nf – and thus its erosion, resembling the effect of chemical cross-linking. Therefore, RSV-ves-nf swells without erosion, leading to stronger mucoadhesion. Similarly, Bełdowski et al. observed that the addition of lipids to high molecular weight hyaluronic acid networks led to a cross-linking-like effect, resulting in appreciably long-lasting systems that might be beneficial in biological systems [82]. Moreover, while the hydration of E-nf might lead to the formation of a tridimensional compact gel, RSV-ves-nf, upon hydration, may form a more loosely structured, continuously hydrated gel-like system in which

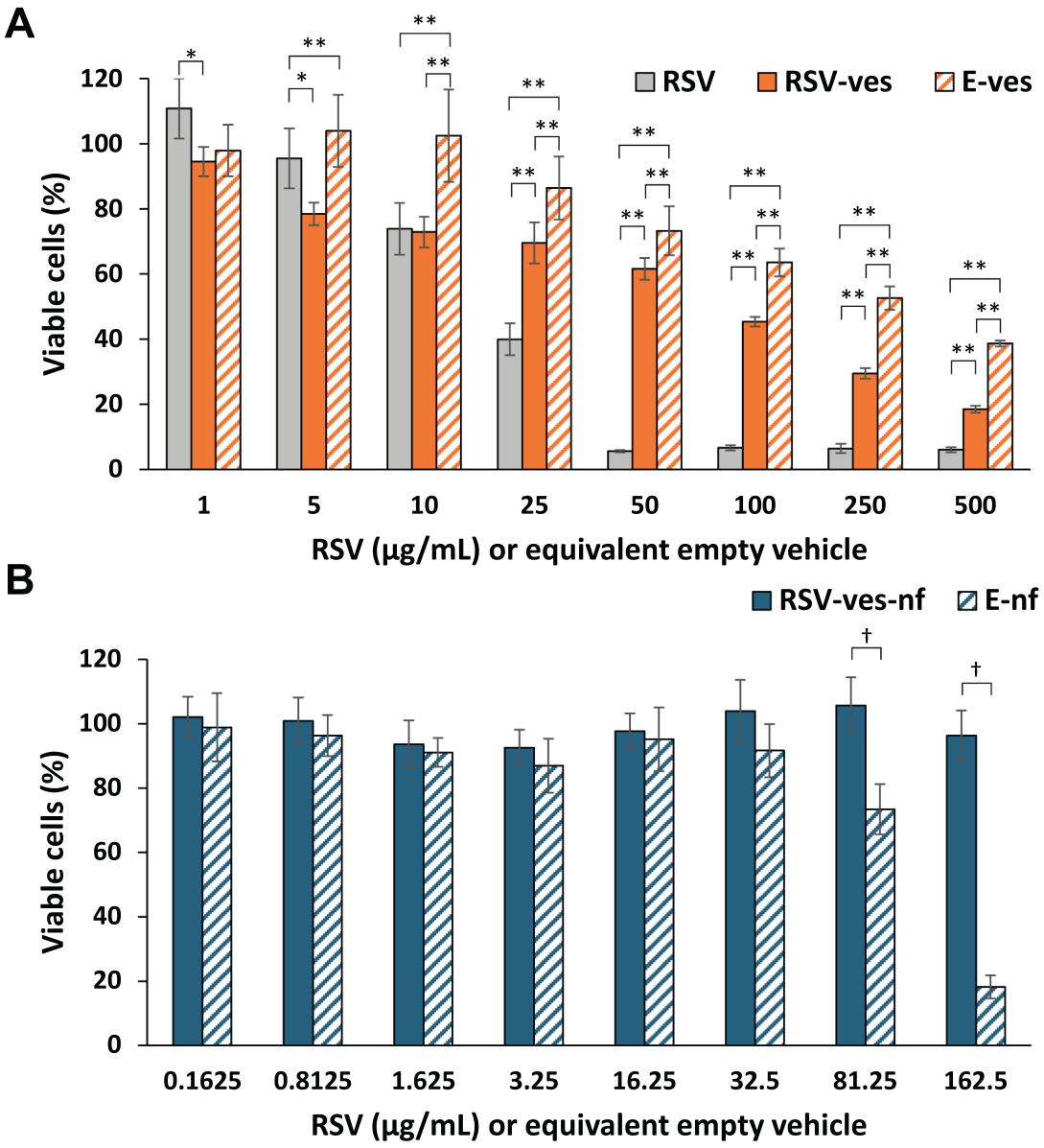

Fig. 6. Biocompatibility of free RSV, RSV-ves and E-ves (A) and RSV-ves-nf and E-nf (B), determined on human keratinocytes upon 24 h exposure to the formulations. Results are expressed as average ± standard deviation of $n = 5$ replicates. Symbols indicate statistically significant difference between groups (* $p < 0.05$ and ** $p < 0.01$, One-way ANOVA with post-hoc Tukey Test; † $p < 0.001$, Student's *t*-test).

the phospholipid vesicles limit the formation of the compact polymer network. This enables deeper interpenetration of alginate chains and mucin, a more favorable contact angle, and ultimately a greater detachment force is required, corresponding to a higher mucoadhesive strength [83]. Kalintas Caglar et al. also observed an increase in the mucoadhesive strength of liposomal black mulberry extract loaded-nanofibers in comparison with empty nanofibers [84].

It should be noted that, while the measured mucoadhesive strength provides solid evidence of the mucoadhesive properties of RSV-ves-nf, correlating these *in vitro* findings to *in vivo* behavior is difficult. To date, the literature does not establish a direct, universal correlation between *in vitro* mucoadhesive strength and *in vivo* nasal retention. Nevertheless, it is known that formulations containing mucoadhesive polymers, such as the alginate used in our study, display increased residence time in the nasal cavity [40,72]. Furthermore, it is reported in the literature that a mucoadhesive strength of 0.3100–0.3800 N is sufficient to allow adhesion to nasal mucosa [85]. Therefore, it could be hypothesized that the mucoadhesive strength measured for RSV-ves-nf, which was approximately 0.76 N/cm^2, could confer extended residence time (>60 min) by resisting the natural mucociliary clearance.

3.6. Biocompatibility

A new formulation, whether it is developed as a medical device or a medicinal product, must comply with high safety standards. Assessing biocompatibility on a relevant cell line is therefore a preliminary requirement for the development of a novel product. To this aim, a human keratinocyte cell line was exposed to the nanofibrous system (RSV-ves-nf) or to its components (RSV, RSV-ves, *E*-nf) to assess their impact on cell metabolic activity *in vitro* (Fig. 6). The free RSV triggered a dose-dependent decrease of the metabolic activity of cells, with a calculated IC_{50} of 17.0 μg/mL that aligns with previous studies performed on the same cell line [86]. Interestingly, vesicular incorporation reduced RSV cytotoxicity, leading to a much higher IC_{50} value (76.7 μg/mL). When the RSV vesicles were embedded in the nanofibers to form the RSV-ves-nf, the RSV cytotoxicity was further reduced, probably due to the controlled release provided by both the vesicles and the polymer network. More specifically, no significant alterations of the cell metabolic activity was observed at any of the tested RSV concentrations, not allowing the calculation of an IC_{50}. The impact of empty vehicles (*E*-ves and E-nf) on cell viability was assessed in parallel, diluting these formulations in a volume of medium that equals the one employed for the corresponding concentration of the RSV-loaded system. Since the *E*-ves and E-nf do not contain RSV, their cytotoxic effect can be better compared to the loaded formulations expressing the IC_{50} as the total concentration of lipids (for vesicles) or polymers (for nanofibers) that leads to a 50% reduction of cell viability (Table 3).

3.7. In vitro antioxidant activity

The upper airways are the outermost region of the respiratory tract, and for their anatomical position and physiological function, they are constantly exposed to environmental pollutants, microorganisms, and xenobiotics. When exposed to these substances/pathogens, the delicate balance between intracellular pro-oxidant and antioxidant factors can be disrupted, leading to oxidative stress and inflammation of the nasal mucosa that compromise its barrier function [4]. Antioxidant agents, such as RSV, can restore this imbalance, limiting the formation of iROS and safeguarding the viability of epithelial cells [87]. In this context, our aim was to assess the ability of RSV-ves-nf to prevent the uncontrolled production of iROS by epithelial cells upon exposure to an external stressor. Briefly, keratinocytes were pre-treated with RSV, RSV formulations or their empty counterparts before exposure to hydrogen peroxide as a pro-oxidant stimulus. The relative abundance of iROS was determined using the DCFH-DA probe, as previously described [44]. The green fluorescent signal produced by the iROS-oxidized sensor was qualitatively monitored by fluorescence microscopy (**Fig. 7 A**), quantified by fluorescence spectroscopy and expressed as a percentage of basal iROS determined in untreated, unstressed cells (**Fig. 7B**). As expected, the free RSV confirmed its well-known antioxidant activity, limiting the iROS generation to a slight increase from the basal level upon exposure to hydrogen peroxide. RSV-ves boosted the antioxidant action of the polyphenol reducing the iROS below the basal level. A contribution from the lipids and other components of the vesicles can be ruled out, as the *E*-ves pre-treatment did not result in a reduction of iROS compared to the untreated, stressed cells ($p > 0.05$). Notably, the nanofibrous system further enhanced the protection from the hydrogen peroxide insult, not only maintaining the homeostasis, but also leading to a reduction of iROS compared to the basal level. Such an effect can be at least partially explained by the presence of sodium alginate in the composition of the nanofibers. In fact, alginate has an intrinsic ability to scavenge hydroxyl and superoxide radicals, which is enhanced for shorter chains polymers [88,89]. The relative contribution of alginate to the reduction of iROS levels can be visualized from the results obtained by treating the cells with E-nf, which highlight a relative iROS concentration of 74 ± 5% compared to untreated cells. Despite the contribution of sodium alginate to the reduction of iROS, it was possible to observe a statistically significant difference ($p < 0.01$) between the effects of E-nf and RSV-ves-nf, highlighting the advantage of the combined system, not only in terms of safety (as previously discussed and shown by Fig. 6B), but also in terms of efficacy.

The mechanisms behind the combined antioxidant activity triggered by RSV and alginate remain to be unveiled; specifically, further investigation will be required to determine whether the observed efficacy stems from additive or synergistic effects. Identifying these interactions will open significant avenues for the design of next-generation bioactive platforms, though such detailed characterization is reserved for subsequent stages of development.

Finally, it should be noted that, while immortalized human keratinocytes are a useful model for the nasal vestibule [90], they only partially reflect the complexity of the respiratory mucosa. Therefore, further validation using primary nasal epithelial cells would be beneficial to support the translation of the proposed technology.

Table 3
IC_{50} of formulations calculated as the concentration of RSV or lipids or polymers (μg/mL) required to reduce HaCaT cell viability by 50%.

	IC_{50} (μg/mL)		
	RSV	Lipids	Polymers
RSV	17.0	–	–
RSV-ves	76.7	1379.9	–
E-ves	–	3914.6	–
E-nf	–	–	3452.2
RSV-ves-nf	>162.5	>2925	>5000

4. Conclusion

In this study, we developed a mucoadhesive nasal patch that combined RSV-loaded phospholipid vesicles with alginate-PEO nanofibers. By addressing RSV poor water solubility through vesicular incorporation and employing a green, aqueous-based electrospinning method, we achieved a biocompatible formulation that exhibited superior mucoadhesion and sustained release compared to the vesicles alone, suggesting that the nanofibrous matrix plays a crucial role in enhancing the interaction with nasal mucosa and modulating RSV release kinetics. However, additional investigation is required to increase the amount of RSV released within a 24-h window and extend the duration of the release studies beyond current timeframe.

Physicochemical analyses provided insight into solid-state behavior and drug-matrix interactions, supporting the stability and compatibility of the components. *In vitro* studies in immortalized human keratinocytes

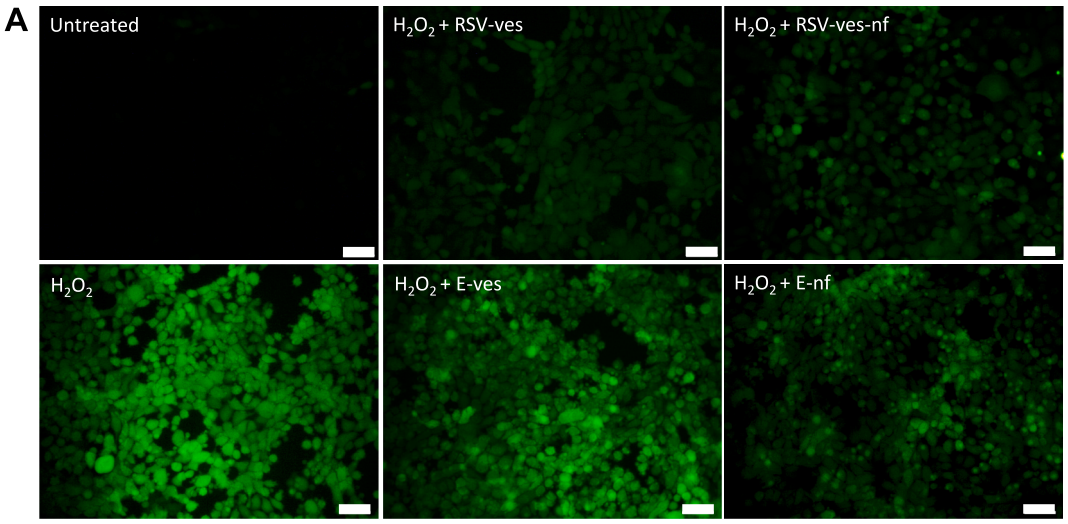

B

Treatment	-	-	RSV	E-ves	RSV-ves	E-nf	RSV-ves-nf
H_2O_2	-	+	+	+	+	+	+
Fluorescence (% of control)	100 ± 8*	240 ± 14	129 ± 10*	202 ± 19	73 ± 7*	74 ± 5*	46 ± 5*†

Fig. 7. iROS levels and antioxidant activity of nanoformulated RSV in keratinocytes. A) representative live cell microscopy images of epithelial cells exposed to the formulations and/or hydrogen peroxide (H_2O_2). The green-fluorescent signal is produced in response to the oxidation of the DCFH-DA sensor by iROS. (Scale bar 50 μm). B) quantification of the intracellular fluorescence intensity after the treatments. Values are reported as average ± standard deviation of 5 replicates, * = $p < 0.01$ *vs.* cells exposed to hydrogen peroxide (H_2O_2) without treatment, † = $p < 0.01$ *vs.* all the other conditions.

confirmed the safety and biological efficacy of the RSV vesicles-in-nanofibers. The observed safety and efficacy offer encouraging preliminary cues, though the translatability in more complex human nasal epithelium models remains to be established.

This study highlights the potential of alginate, that played a central role in ensuring biocompatibility and strong interaction with nasal mucosa, underscoring the value of natural polymers in the development of safe and effective mucosal delivery systems. The embedding of phospholipid vesicles within alginate-based nanofibers proved to be a strategy that merges the benefits of each system into a single platform capable of overcoming conventional delivery barriers, supporting our original hypothesis. This eco-friendly, nanotechnology-based strategy offers new perspectives on nasal delivery, particularly for bioactive compounds with solubility and stability limitations. Although the present findings provide key foundational knowledge on the proposed RSV vesicles-in-nanofibers, *in vivo* studies will be vital for assessing the pharmacokinetic profile, residence time, dosing regimen, therapeutic efficacy, and clinical applicability.

CRediT authorship contribution statement

Luca Casula: Writing – review & editing, Writing – original draft, Validation, Methodology, Investigation, Formal analysis, Data curation, Conceptualization. **Michele Schlich:** Writing – review & editing, Methodology, Investigation, Data curation. **Elena Pini:** Methodology, Investigation, Data curation. **Giovanna Rassu:** Methodology, Investigation, Data curation. **Elena Bellotti:** Methodology, Investigation, Data curation. **Francesco Lai:** Validation, Supervision, Methodology. **Maria Cristina Cardia:** Methodology, Investigation. **Salvatore Marceddu:** Investigation. **Aurélien Dupont:** Investigation. **Chiara Sinico:** Validation, Supervision, Data curation. **Carla Caddeo:** Writing – review & editing, Writing – original draft, Supervision, Project administration, Investigation, Funding acquisition, Conceptualization.

Funding

This work was supported by UniCA-Progetti biennali di Ateneo Finanziati dalla Fondazione di Sardegna 2021 (CUP F73C22001170007).

Declaration of competing interest

The authors declare that they have no known competing financial interests or personal relationships that could have appeared to influence the work reported in this paper.

Acknowledgments

The EDUC-Share project, funded by the European Union's Horizon 2020 research and innovation program under grant agreement No. 101017526, is gratefully acknowledged for financial support for the cryo-TEM measurements taken at the UNIVREN-BIOSIT-MRic core facility at the University of Rennes (France). The authors would like to thank Prof. Caterina Cristallini for the fruitful discussion regarding the characterization data of sodium alginate.

Appendix A. Supplementary data

Supplementary data to this article can be found online at https://doi.org/10.1016/j.ijbiomac.2026.152376.

Data availability

Data will be made available on request.

References

[1] G. Valacchi, F. Virgili, C. Cervellati, A. Pecorelli, OxInflammation: From subclinical condition to pathological biomarker, Front. Physiol. 9 (2018) 385233, https://doi.org/10.3389/fphys.2018.00858.

[2] J. Zhou, J. Zhou, R. Liu, Y. Liu, J. Meng, Q. Wen, Y. Luo, S. Liu, H. Li, L. Ba, J. Du, The oxidant-antioxidant imbalance was involved in the pathogenesis of chronic rhinosinusitis with nasal polyps, Front. Immunol. 15 (2024) 1380846, https://doi.org/10.3389/fimmu.2024.1380846.

[3] L. Meng, S. Liu, J. Luo, Y. Tu, T. Li, P. Li, J. Yu, L. Shi, Oxidative stress and reactive oxygen species in otorhinolaryngological diseases: insights from pathophysiology to targeted antioxidant therapies, Redox Rep. 30 (2025) 2458942, https://doi.org/10.1080/13510002.2025.2458942.

[4] J. Tai, J.M. Shin, J. Park, M. Han, T.H. Kim, Oxidative Stress and Antioxidants in Chronic Rhinosinusitis with Nasal Polyps, Antioxidants 12 (2023) 195, https://doi.org/10.3390/antiox12010195.

[5] S.W. Kim, D.W. Kim, R. Khalmuratova, J.H. Kim, M.H. Jung, D.Y. Chang, E.C. Shin, H.K. Lee, H.W. Shin, C.S. Rhee, S.Y. Jeon, Y.G. Min, Resveratrol prevents development of eosinophilic rhinosinusitis with nasal polyps in a mouse model, Allergy Eur. J. Allergy Clin. Immunol 68 (2013) 862–869, https://doi.org/10.1111/all.12132.

[6] W. Zhang, R. Tang, G. Ba, M. Li, H. Lin, Anti-allergic and anti-inflammatory effects of resveratrol via inhibiting TXNIP-oxidative stress pathway in a mouse model of allergic rhinitis, World Allergy Organ. J. 13 (2020) 100473, https://doi.org/10.1016/j.waojou.2020.100473.

[7] C. Lv, Y. Zhang, L. Shen, Preliminary Clinical Effect Evaluation of Resveratrol in Adults with Allergic Rhinitis, Int. Arch. Allergy Immunol. 175 (2018) 231–236, https://doi.org/10.1159/000486959.

[8] P. Mastromarino, D. Capobianco, F. Cannata, C. Nardis, E. Mattia, A. De Leo, R. Restignoli, A. Francioso, L. Mosca, Resveratrol inhibits rhinovirus replication and expression of inflammatory mediators in nasal epithelia, Antivir. Res. 123 (2015) 15–21, https://doi.org/10.1016/j.antiviral.2015.08.010.

[9] N.S. Alexander, N. Hatch, S. Zhang, D. Skinner, J. Fortenberry, E.J. Sorscher, B. A. Woodworth, Resveratrol has salutary effects on mucociliary transport and inflammation in sinonasal epithelium, Laryngoscope 121 (2011) 1313–1319, https://doi.org/10.1002/lary.21798.

[10] E. Marttin, N.G.M. Schipper, J. Coos Verhoef, F.W.H.M. Merkus, Nasal mucociliary clearance as a factor in nasal drug delivery, Adv. Drug Deliv. Rev. 29 (1998) 13–38, https://doi.org/10.1016/S0169-409X(97)00059-8.

[11] M.I. Ugwoke, R.U. Agu, N. Verbeke, R. Kinget, Nasal mucoadhesive drug delivery: Background, applications, trends and future perspectives, Adv. Drug Deliv. Rev. 57 (2005) 1640–1665, https://doi.org/10.1016/j.addr.2005.07.009.

[12] B. Chatterjee, N. Amalina, P. Sengupta, U.K. Mandal, Mucoadhesive Polymers and Their Mode of Action: A Recent Update, J. Appl. Pharm. Sci. 7 (2017) 195–203, https://doi.org/10.7324/JAPS.2017.70533.

[13] R. Scherließ, Nasal Formulations for Drug Administration and Characterization of Nasal Preparations in Drug Delivery, Ther. Deliv. 11 (2020) 183–191, https://doi.org/10.4155/TDE-2019-0086.

[14] J.D. Smart, The basics and underlying mechanisms of mucoadhesion, Adv. Drug Deliv. Rev. 57 (2005) 1556–1568, https://doi.org/10.1016/J.ADDR.2005.07.001.

[15] H.S. Sofi, A. Abdal-hay, S. Ivanovski, Y.S. Zhang, F.A. Sheikh, Electrospun nanofibers for the delivery of active drugs through nasal, oral and vaginal mucosa: Current status and future perspectives, Mater. Sci. Eng. C 111 (2020) 110756, https://doi.org/10.1016/j.msec.2020.110756.

[16] B.J. Dukovski, I. Plantić, I. Čunčić, I. Krtalić, M. Juretić, I. Pepić, J. Lovrić, A. Hafner, Lipid/alginate nanoparticle-loaded in situ gelling system tailored for dexamethasone nasal delivery, Int. J. Pharm. 533 (2017) 480–487, https://doi.org/10.1016/j.ijpharm.2017.05.065.

[17] S. Dehghan, M.T. Kheiri, K. Abnous, M. Eskandari, M. Tafaghodi, Preparation, characterization and immunological evaluation of alginate nanoparticles loaded with whole inactivated influenza virus: Dry powder formulation for nasal immunization in rabbits, Microb. Pathog. 115 (2018) 74–85, https://doi.org/10.1016/j.micpath.2017.12.011.

[18] S.B. Patil, K.K. Sawant, Development, optimization and *in vitro* evaluation of alginate mucoadhesive microspheres of carvedilol for nasal delivery, J. Microencapsul. 26 (2009) 432–443, https://doi.org/10.1080/02652040802456726.

[19] K.P. Alcantara, N. Nalinratana, N. Chutiwitoonchai, A.L. Castillo, W. Banlunara, O. Vajragupta, P. Rojsitthisak, P. Rojsitthisak, Enhanced nasal deposition and anti-Coronavirus effect of Favipiravir-loaded mucoadhesive Chitosan–Alginate nanoparticles, Pharmaceutics 14 (2022), https://doi.org/10.3390/pharmaceutics14122680.

[20] N. Hussein, H. Omer, A. Ismael, M. Albed Alhnan, A. Elhissi, W. Ahmed, Spray-dried alginate microparticles for potential intranasal delivery of ropinirole hydrochloride: development, characterization and histopathological evaluation, Pharm. Dev. Technol. 25 (2020) 290–299, https://doi.org/10.1080/10837450.2019.1567762.

[21] P.S. Rajinikanth, C. Sankar, B. Mishra, Sodium alginate microspheres of metoprolol tartrate for intranasal systemic delivery: development and evaluation, Drug Deliv. 10 (2003) 21–28, https://doi.org/10.1080/713840323.

[22] N.K. Grilc, A. Zidar, P. Kocbek, T. Rijavec, T. Colja, A. Lapanje, M. Jeras, M. Gobec, I. Mlinarič-Raščan, M. Gašperlin, J. Kristl, Š. Zupančič, Nanofibers with genotyped Bacillus strains exhibiting antibacterial and immunomodulatory activity, J. Control. Release 355 (2023) 371–384, https://doi.org/10.1016/J.JCONREL.2023.01.082.

[23] P. Wen, K. Feng, H. Yang, X. Huang, M.H. Zong, W.Y. Lou, N. Li, H. Wu, Electrospun core-shell structured nanofilm as a novel colon-specific delivery system for protein, Carbohydr. Polym. 169 (2017) 157–166, https://doi.org/10.1016/j.carbpol.2017.03.082.

[24] C.A. Bonino, M.D. Krebs, C.D. Saquing, S.I. Jeong, K.L. Shearer, E. Alsberg, S. A. Khan, Electrospinning alginate-based nanofibers: From blends to crosslinked low molecular weight alginate-only systems, Carbohydr. Polym. 85 (2011) 111–119, https://doi.org/10.1016/j.carbpol.2011.02.002.

[25] Y. Tang, X. Lan, C. Liang, Z. Zhong, R. Xie, Y. Zhou, X. Miao, H. Wang, W. Wang, Honey loaded alginate/PVA nanofibrous membrane as potential bioactive wound dressing, Carbohydr. Polym. 219 (2019) 113–120, https://doi.org/10.1016/j.carbpol.2019.05.004.

[26] D. Jahantigh, M. Saadati, M. Fasihi Ramandi, M. Mousavi, A.M. Zand, Novel intranasal vaccine delivery system by chitosan nanofibrous membrane containing N-terminal region of IpaD antigen as a nasal shigellosis vaccine, studies in Guinea pigs, J. Drug Delivery Sci. Technol. 24 (2014) 33–39, https://doi.org/10.1016/S1773-2247(14)50005-6.

[27] E. Taha, S.A. Nour, W. Mamdouh, M.J. Naguib, Investigating the potential of highly porous zopiclone-loaded 3D electrospun nanofibers for brain targeting via the intranasal route, Int. J. Pharm. 660 (2024) 124230, https://doi.org/10.1016/j.ijpharm.2024.124230.

[28] K. Chachlioutaki, M. Liogka, P.M. Petinari, S. Koltsakidis, A. Papadimitriou-Tsantarliotou, C. Bekiari, I.S. Vizirianakis, D. Tzetzis, N. Bouropoulos, D. G. Fatouros, Electrospun mucoadhesive nanofibrous films for intranasal delivery of propranolol hydrochloride for migraine prophylaxis, J. Drug Delivery Sci. Technol. 114 (2025) 107552, https://doi.org/10.1016/j.jddst.2025.107552.

[29] H. Elnahas, L. Materon, R. Tiwari, M.M. Yallapu, V. Padilla, K. Lozano, Pullulan-based nanofiber membranes with antibacterial and anti-inflammatory properties for rhinosinusitis therapy, Ther. Deliv. (2026), https://doi.org/10.1080/20415990.2026.2629205.

[30] G.G. Rivelli, A.C. Perez, P.H.R. Silva, E.C. de L. Gomes, C.P. de S. Moreira, E. Tamashiro, F.C.P. Valera, W.T. Anselmo-Lima, G.A. Pianetti, A. Silva-Cunha, Biodegradable electrospun nanofibers: a new approach for rhinosinusitis treatment, Eur. J. Pharm. Sci. 163 (2021) 1–11, https://doi.org/10.1016/j.ejps.2021.105852.

[31] R. Krishnan, S. Sundarrajan, S. Ramakrishna, Green processing of nanofibers for regenerative medicine, Macromol. Mater. Eng. 298 (2013) 1034–1058, https://doi.org/10.1002/mame.201200323.

[32] H.A. Abboud, R. Zelkó, A. Kazsoki, A systematic review of liposomal nanofibrous scaffolds as a drug delivery system: a decade of progress in controlled release and therapeutic efficacy, Drug Deliv. 32 (2025), https://doi.org/10.1080/10717544.2024.2445259.

[33] L. Casula, A. Zidar, J. Kristl, M. Jeras, S. Kralj, A.M. Fadda, Š. Zupančič, Development of nanofibers with embedded liposomes containing an immunomodulatory drug using green electrospinning, Pharmaceutics 15 (4) (2023) 1245, https://doi.org/10.3390/PHARMACEUTICS15041245.

[34] L. Casula, S. Demuro, R. Argenziano, F. Pintus, C. Caddeo, A. Napolitano, Phospholipid vesicle-based formulation to unlock the potential of a biosynthetic melanin: a strategy to overcome the insolubility barriers, J. Drug Delivery Sci. Technol. 113 (2025), https://doi.org/10.1016/j.jddst.2025.107390.

[35] C. Caddeo, D. Lucchesi, X. Fernàndez-Busquets, D. Valenti, G. Penno, A.M. Fadda, L. Pucci, Efficacy of a resveratrol nanoformulation based on a commercially available liposomal platform, Int. J. Pharm. 608 (2021) 121086, https://doi.org/10.1016/j.ijpharm.2021.121086.

[36] Š. Zupančič, L. Casula, T. Rijavec, A. Lapanje, M. Luštrik, A.M. Fadda, P. Kocbek, J. Kristl, Sustained release of antimicrobials from double-layer nanofiber mats for local treatment of periodontal disease, evaluated using a new micro flow-through apparatus, J. Control. Release 316 (2019) 223–235, https://doi.org/10.1016/j.jconrel.2019.10.008.

[37] K. Sakugawa, A. Ikeda, A. Takemura, H. Ono, Simplified method for estimation of composition of alginates by FTIR, J. Appl. Polym. Sci. 93 (2004) 1372–1377, https://doi.org/10.1002/app.20589.

[38] F.N.S. Fachel, B. Medeiros-Neves, M. Dal Prá, R.S. Schuh, K.S. Veras, V.L. Bassani, L.S. Koester, A.T. Henriques, E. Braganhol, H.F. Teixeira, Box-Behnken design optimization of mucoadhesive chitosan-coated nanoemulsions for rosmarinic acid nasal delivery—In vitro studies, Carbohydr. Polym. 199 (2018) 572–582, https://doi.org/10.1016/j.carbpol.2018.07.054.

[39] V.M. Leitner, D. Guggi, A.H. Krauland, A. Bernkop-Schnärch, Nasal delivery of human growth hormone: In vitro and in vivo evaluation of a thiomer/glutathione microparticulate delivery system, J. Control. Release 100 (2004) 87–95, https://doi.org/10.1016/j.jconrel.2004.08.001.

[40] M. Trenkel, R. Scherließ, Nasal powder formulations: In-vitro characterisation of the impact of powders on nasal residence time and sensory effects, Pharmaceutics 13 (2021), https://doi.org/10.3390/pharmaceutics13030385.

[41] P. Vashisth, V. Pruthi, Synthesis and characterization of crosslinked gellan/PVA nanofibers for tissue engineering application, Mater. Sci. Eng. C 67 (2016) 304–312, https://doi.org/10.1016/j.msec.2016.05.049.

[42] R. Lombardo, M. Ruponen, J. Rautio, R. Lampinen, K.M. Kanninen, A.M. Koivisto, E. Penttilä, H. Löppönen, S. Demartis, P. Giunchedi, G. Rassu, M.E. Fragalà, R. Pignatello, Corrigendum to "A technological comparison of freeze-dried poly-ε-caprolactone (PCL) and poly (lactic-co-glycolic acid) (PLGA) nanoparticles loaded with clozapine for nose-to-brain delivery" [J. Drug Deliv. Sci. Technol. 93 (March 2024), 105419], J. Drug Delivery Sci. Technol. 94 (2024) 105518, https://doi.org/10.1016/j.jddst.2024.105518.

[43] R. Lombardo, M. Ruponen, J. Rautio, R. Lampinen, K.M. Kanninen, A.M. Koivisto, E. Penttilä, H. Löppönen, S. Demartis, P. Giunchedi, G. Rassu, M.E. Fragalà, R. Pignatello, A technological comparison of freeze-dried poly-ε-caprolactone (PCL) and poly (lactic-co-glycolic acid) (PLGA) nanoparticles loaded with clozapine for nose-to-brain delivery, J. Drug Delivery Sci. Technol. 93 (2024), https://doi.org/10.1016/j.jddst.2024.105419.

[44] C. Ilgaz, L. Casula, G. Sarais, M. Schlich, D. Dessì, M. Cristina, C. Sinico, P. Kadiroglu, F. Lai, M.C. Cardia, C. Sinico, P. Kadiroglu, F. Lai, Proniosomal

encapsulation of olive leaf extract for improved delivery of oleuropein : Towards the valorization of an agro-industrial byproduct, Food Chem. 479 (2025) 143877, https://doi.org/10.1016/j.foodchem.2025.143877.
[45] C. Indolfi, C. Mignini, F. Valitutti, I. Bizzarri, G. Dinardo, A. Klain, M. Miraglia del Giudice, G. Di Cara, Effects of nasal solution incorporating resveratrol and carboxymethyl-B-glucan in preschool non-atopic children with wheezing, Nutrients 16 (2024) 2197, https://doi.org/10.3390/nu16142197.
[46] I. Martignoni, V. Trotta, W.H. Lee, C.Y. Loo, M. Pozzoli, P.M. Young, S. Scalia, D. Traini, Resveratrol solid lipid microparticles as dry powder formulation for nasal delivery, characterization and in vitro deposition study, J. Microencapsul. 33 (2016) 735–742, https://doi.org/10.1080/02652048.2016.1260659.
[47] P. Lin, G. Thirumugam, T. Manickam, G. Dharman, K. Jayaprakasam, Long-acting injectable nanoemulsion for anti-inflammatory therapy: luteolin and resveratrol-loaded CMC formulation regulates TH1/TH2 homeostasis in ovalbumin-induced allergic rhinitis in mice models, RSC Adv. 15 (2025) 35022–35035, https://doi.org/10.1039/d5ra03121d.
[48] Y. Kim, S. Hwang, R. Khalmuratova, S. Kang, M. Lee, Y. Song, J.W. Park, J. Yu, H. W. Shin, Y. Lee, α-Helical cell-penetrating peptide-mediated nasal delivery of resveratrol for inhibition of epithelial-to-mesenchymal transition, J. Control. Release 317 (2020) 181–194, https://doi.org/10.1016/j.jconrel.2019.11.034.
[49] A. Ahad, A.A. Al-Saleh, A.M. Al-Mohizea, F.I. Al-Jenoobi, M. Raish, A.E.B. Yassin, M.A. Alam, Formulation and characterization of Phospholipon 90 G and tween 80 based transfersomes for transdermal delivery of eprosartan mesylate, Pharm. Dev. Technol. 23 (2018) 787–793, https://doi.org/10.1080/10837450.2017.1330345.
[50] C. Wu, H. Wang, J. Cao, Tween-80 improves single/coaxial electrospinning of three-layered bioartificial blood vessel, J. Mater. Sci. Mater. Med. 34 (2023) 1–15, https://doi.org/10.1007/s10856-022-06707-x.
[51] C. Zhuang, Y. Jiang, Y. Zhong, Y. Zhao, Y. Deng, J. Yue, D. Wang, S. Jiao, H. Gao, H. Chen, H. Mu, Development and characterization of nano-bilayer films composed of polyvinyl alcohol, chitosan and alginate, Food Control 86 (2018) 191–199, https://doi.org/10.1016/j.foodcont.2017.11.024.
[52] M.R. Vijayakumar, K.Y. Vajanthri, C.K. Balavigneswaran, S.K. Mahto, N. Mishra, M.S. Muthu, S. Singh, Pharmacokinetics, biodistribution, in vitro cytotoxicity and biocompatibility of Vitamin E TPGS coated trans resveratrol liposomes, Colloid Surf. B-Biointerfaces 145 (2016) 479–491, https://doi.org/10.1016/j.colsurfb.2016.05.037.
[53] K. Vanaja, M.A. Wahl, L. Bukarica, H. Heinle, Liposomes as carriers of the lipid soluble antioxidant resveratrol: Evaluation of amelioration of oxidative stress by additional antioxidant vitamin, Life Sci. 93 (2013) 917–923, https://doi.org/10.1016/j.lfs.2013.10.019.
[54] C. Mormile, O. Opriș, S. Bellucci, I. Lung, I. Kacso, A. Turza, A. Stegarescu, S. Tripon, M.L. Soran, I. Băldea, Natrium Alginate and Graphene Nanoplatelets-Based Efficient Material for Resveratrol Delivery, Gels 11 (2025) 15, https://doi.org/10.3390/gels11010015.
[55] B. Balanč, K. Trifković, V. Đorđević, S. Marković, R. Pjanović, V. Nedović, B. Bugarski, Novel resveratrol delivery systems based on alginate-sucrose and alginate-chitosan microbeads containing liposomes, Food Hydrocoll. 61 (2016) 832–842, https://doi.org/10.1016/j.foodhyd.2016.07.005.
[56] Y. Iqbal, F. Amin, M.H. Aziz, H.A. Alhadlaq, Z.A.M. Alaizeri, Biomimetic sodium alginate functionalized gold nanoparticles loaded with Trans-resveratrol for in-vitro cancer treatment and intercellular ROS studies against MCF-7 cell lines, Colloids Surfaces A Physicochem. Eng. Asp. 712 (2025) 136448, https://doi.org/10.1016/j.colsurfa.2025.136448.
[57] J. Mirtič, H. Balažic, Š. Zupančič, J. Kristl, Effect of solution composition variables on electrospun alginate nanofibers: Response surface analysis, Polymers (Basel). 11 (2019) 692, https://doi.org/10.3390/polym11040692.
[58] O. Husain, W. Lau, M. Edirisinghe, M. Parhizkar, Investigating the particle to fibre transition threshold during electrohydrodynamic atomization of a polymer solution, Mater. Sci. Eng. C 65 (2016) 240–250, https://doi.org/10.1016/j.msec.2016.03.076.
[59] S.I. Jeong, M.D. Krebs, C.A. Bonino, S.A. Khan, E. Alsberg, Electrospun alginate nanofibers with controlled cell adhesion for tissue engineering, Macromol. Biosci. 10 (2010) 934–943, https://doi.org/10.1002/mabi.201000046.
[60] B. Ghorani, A. Alehosseini, N. Tucker, Nanocapsule formation by electrospinning, Elsevier Inc., 2017, https://doi.org/10.1016/B978-0-12-809436-5.00008-2.
[61] S.L. Shenoy, W.D. Bates, H.L. Frisch, G.E. Wnek, Role of chain entanglements on fiber formation during electrospinning of polymer solutions: Good solvent, non-specific polymer-polymer interaction limit, Polymer (Guildf). 46 (2005) 3372–3384, https://doi.org/10.1016/j.polymer.2005.03.011.
[62] R.H. De Freitas Zômpero, A. López-Rubio, S.C. de Pinho, J.M. Lagaron, L.G. de la Torre, Hybrid encapsulation structures based on β-carotene-loaded nanoliposomes within electrospun fibers, Colloid Surf. B-Biointerfaces 134 (2015) 475–482, https://doi.org/10.1016/j.colsurfb.2015.03.015.
[63] M. Schlich, F. Lai, R. Pireddu, E. Pini, G. Ailuno, A.M. Fadda, D. Valenti, C. Sinico, Resveratrol proniosomes as a convenient nanoingredient for functional food, Food Chem. 310 (2020) 125950, https://doi.org/10.1016/j.foodchem.2019.125950.
[64] M. Aprilliza Helmiyati, Characterization and properties of sodium alginate from brown algae used as an ecofriendly superabsorbent, in: IOP Conf. Ser. Mater. Sci, IOP Publishing, Eng, 2017 012019, https://doi.org/10.1088/1757-899X/188/1/012019.
[65] L. Casula, M. Schlich, M.C. Cardia, E. Lai, S. Marceddu, R. Pireddu, D. Valenti, C. Sinico, F. Lai, E. Pini, Design and Bottom-up Production of an Aerosolizable Cannabidiol Nanosuspension, Mol. Pharm. 22 (2025) 498–508, https://doi.org/10.1021/acs.molpharmaceut.4c01095.
[66] N.S. Vrandečić, M. Erceg, M. Jakić, I. Klarić, Kinetic analysis of thermal degradation of poly(ethylene glycol) and poly(ethylene oxide)s of different molecular weight, Thermochim. Acta 498 (2010) 71–80, https://doi.org/10.1016/J.TCA.2009.10.005.
[67] R. Sun, G. Zhao, S. Ni, Q. Xia, Lipid based nanocarriers with different lipid compositions for topical delivery of resveratrol: comparative analysis of characteristics and performance, J. Drug Delivery Sci. Technol. 24 (2014) 591–600, https://doi.org/10.1016/S1773-2247(14)50124-4.
[68] S.R. Abulateefeh, M.O. Taha, Enhanced drug encapsulation and extended release profiles of calcium–alginate nanoparticles by using tannic acid as a bridging cross-linking agent, J. Microencapsul. 32 (2015) 96–105, https://doi.org/10.3109/02652048.2014.985343.
[69] G. Davidov-Pardo, D.J. McClements, Resveratrol encapsulation: Designing delivery systems to overcome solubility, stability and bioavailability issues, Trends Food Sci. Technol. 38 (2014) 88–103, https://doi.org/10.1016/j.tifs.2014.05.003.
[70] C. Sinico, R. Pireddu, E. Pini, D. Valenti, C. Caddeo, A.M. Fadda, F. Lai, Enhancing Topical Delivery of Resveratrol through a Nanosizing Approach, Planta Med. 83 (2017) 476–481, https://doi.org/10.1055/s-0042-103688.
[71] M. Jug, A. Hafner, J. Lovrić, M.L. Kregar, I. Pepić, Ž. Vanić, B. Cetina-Čižmek, J. Filipović-Grčić, An overview of in vitro dissolution/release methods for novel mucosal drug delivery systems, J. Pharm. Biomed. Anal. 147 (2018) 350–366, https://doi.org/10.1016/j.jpba.2017.06.072.
[72] D. Inoue, Y. Seto, H. To, Nasal residence depending on the administered dosage form: impact of formulation type on the in vivo nasal retention time of drugs in rats, Pharmaceutics 17 (2025) 863, https://doi.org/10.3390/pharmaceutics17070863.
[73] A. Shilpa, S.S. Agrawal, A.R. Ray, Controlled delivery of drugs from alginate matrix, J. Macromol. Sci. Polym. Rev. 43 (2003) 187–221, https://doi.org/10.1081/MC-120020160.
[74] D. Inoue, A. Tanaka, S. Kimura, A. Kiriyama, H. Katsumi, A. Yamamoto, K. ichi Ogawara, T. Kimura, K. Higaki, R. Yutani, T. Sakane, T. Furubayashi, The relationship between in vivo nasal drug clearance and in vitro nasal mucociliary clearance: application to the prediction of nasal drug absorption, Eur. J. Pharm. Sci. 117 (2018) 21–26, https://doi.org/10.1016/J.EJPS.2018.01.032.
[75] M.I. Ugwoke, N. Verbeke, R. Kinget, The biopharmaceutical aspects of nasal mucoadhesive drug delivery, J. Pharm. Pharmacol. 53 (2010) 3–21, https://doi.org/10.1211/0022357011775145.
[76] M.C. Cardia, C. Caddeo, F. Lai, A.M. Fadda, C. Sinico, M. Luhmer, 1H NMR study of the interaction of trans-resveratrol with soybean phosphatidylcholine liposomes, Sci. Rep. 9 (2019) 17736, https://doi.org/10.1038/s41598-019-54199-7.
[77] Y. Ge, J. Tang, H. Fu, Y. Fu, Y. Wu, Characteristics, Controlled-release and Antimicrobial Properties of Tea Tree Oil Liposomes-incorporated Chitosan-based Electrospun Nanofiber Mats, Fibers Polym. 20 (2019) 698–708, https://doi.org/10.1007/s12221-019-1092-1.
[78] N. Monteiro, M. Martins, A. Martins, N.A. Fonseca, J.N. Moreira, R.L. Reis, N. M. Neves, Antibacterial activity of chitosan nanofiber meshes with liposomes immobilized releasing gentamicin, Acta Biomater. 18 (2015) 196–205, https://doi.org/10.1016/j.actbio.2015.02.018.
[79] D.G. Yu, C. Branford-White, G.R. Williams, S.W.A. Bligh, K. White, L.M. Zhu, N. P. Chatterton, Self-assembled liposomes from amphiphilic electrospun nanofibers, Soft Matter 7 (2011) 8239–8247, https://doi.org/10.1039/C1SM05961K.
[80] S. Chung, J.M. Peters, K. Detyniecki, W. Tatum, A.L. Rabinowicz, E. Carrazana, The nose has it: Opportunities and challenges for intranasal drug administration for neurologic conditions including seizure clusters, Epilepsy Behav. Reports 21 (2023) 100581, https://doi.org/10.1016/j.ebr.2022.100581.
[81] A. Bartkowiak, M. Rojewska, K. Hyla, J. Zembrzuska, K. Prochaska, Surface and swelling properties of mucoadhesive blends and their ability to release fluconazole in a mucin environment, Colloid Surf. B-Biointerfaces 172 (2018) 586–593, https://doi.org/10.1016/J.COLSURFB.2018.09.014.
[82] P. Bełdowski, P. Weber, A. Dedinaite, P.M. Claesson, A. Gadomski, Physical crosslinking of hyaluronic acid in the presence of phospholipids in an aqueous nano-environment, Soft Matter 14 (2018) 8997–9004, https://doi.org/10.1039/C8SM01388H.
[83] C.S.A. de Lima, J.P.R.O. Varca, V.M. Alves, K.M. Nogueira, C.P.C. Cruz, M.I. Rial-Hermida, S.S. Kadłubowski, G.H.C. Varca, A.B. Lugão, Mucoadhesive Polymers and Their Applications in Drug Delivery Systems for the Treatment of Bladder Cancer, Gels 8 (2022) 587, https://doi.org/10.3390/gels8090587.
[84] N. Kalintas Caglar, O. Saroglu, C.Y. Karakas, C.O. Tasci, G. Catalkaya, R. M. Yildirim, E.E. Gultepe, S. Gulec, O. Sagdic, E. Capanoglu, A. Karadag, Liposomal black mulberry extract loaded-nanofibers: preparation, characterisation, and bioaccessibility of phenolics by simulated in vitro digestion combined with the Caco-2 cell model, Int. J. Food Sci. Technol. 59 (2024) 9298–9309, https://doi.org/10.1111/IJFS.17570.
[85] K. Suhagiya, C.H. Borkhataria, S. Gohil, R.A. Manek, K.A. Patel, N.K. Patel, D. V. Patel, Development of mucoadhesive in-situ nasal gel formulation for enhanced bioavailability and efficacy of rizatriptan in migraine treatment, Results Chem. 6 (2023) 101010, https://doi.org/10.1016/J.RECHEM.2023.101010.
[86] M. Bostan, M. Mihaila, G.G. Petrica-Matei, N. Radu, R. Hainarosie, C.D. Stefanescu, V. Roman, C.C. Diaconu, Resveratrol modulation of apoptosis and cell cycle response to Cisplatin in head and neck cancer cell lines, Int. J. Mol. Sci. 2021 22 (22) (2021) 6322, https://doi.org/10.3390/IJMS22126322, 6322.
[87] Z. Zhang, M. Ge, D. Wu, W. Li, W. Chen, P. Liu, H. Zhang, Y. Yang, Resveratrol-loaded sulfated Hericium erinaceus β-glucan-chitosan nanoparticles: Preparation, characterization and synergistic anti-inflammatory effects, Carbohydr. Polym. 332 (2024) 121916, https://doi.org/10.1016/J.CARBPOL.2024.121916.
[88] S.M. Elbayomi, H. Wang, T.M. Tamer, Y. You, Enhancement of antioxidant and hydrophobic properties of Alginate via aromatic derivatization: preparation,

characterization, and evaluation, Polymers 2021 13 (13) (2021) 2575, https://doi.org/10.3390/POLYM13152575, 2575.

[89] M. Falkeborg, L.Z. Cheong, C. Gianfico, K.M. Sztukiel, K. Kristensen, M. Glasius, X. Xu, Z. Guo, Alginate oligosaccharides: Enzymatic preparation and antioxidant property evaluation, Food Chem. 164 (2014) 185–194, https://doi.org/10.1016/J.FOODCHEM.2014.05.053.

[90] M.F. Morgene, C. Maurin, S. Pillet, P. Berthelot, F. Morfin, B. Pozzetto, E. Botelho-Nevers, P.O. Verhoeven, HaCaT epithelial cells as an innovative novel model of rhinovirus infection and impact of clarithromycin treatment on infection kinetics, Virology 523 (2018) 27–34, https://doi.org/10.1016/j.virol.2018.07.025.